Contents lists available at ScienceDirect

Journal of Colloid and Interface Science

journal homepage: www.elsevier.com/locate/jcis



Regular Article

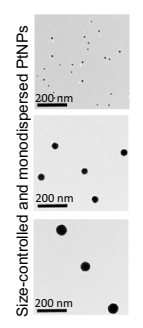
Synthesis, characterization, and environmental behaviors of monodispersed platinum nanoparticles

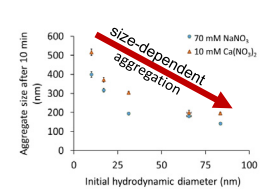


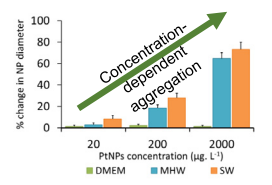
Mithun Sikder a,b, Jingjing Wang a,b, G. Thomas Chandler b, Debora Berti c, Mohammed Baalousha a,b,*

- a South Carolina SmartState Center for Environmental Nanoscience and Risk (CENR). Arnold School of Public Health. University of South Carolina. Columbia. SC 29208. USA
- b Department of Environmental Health Sciences, Arnold School of Public Health, University of South Carolina, Columbia, SC 29208, USA
- ^c National Center for Earth and Environmental Nanotechnology Infrastructure (NanoEarth), Virginia Tech, 24061, USA

GRAPHICAL ABSTRACT







ARTICLE INFO

Article history: Received 14 November 2018 Revised 7 January 2019 Accepted 10 January 2019 Available online 11 January 2019

Keywords: Platinum nanoparticle Seed mediated growth Multimethod characterization Aggregation kinetics (Eco)toxicological media Colloidal stability of nanoparticles

ABSTRACT

The release of platinum group elements, including platinum nanoparticles (PtNPs), has been increasing over recent decades. However, few studies have investigated the fate, behavior and effects of PtNPs in environmental media. Here, we report a protocol for the synthesis of five different sizes $(8.5 \pm 1.2,$ 10.3 ± 1.3 , 20.0 ± 4.8 , 40.5 ± 4.1 , and 70.8 ± 4.2 nm) of monodispersed citrate- and polyvinylpyrrolidone (PVP)-coated PtNPs, together with a characterization of their behaviors using a multi method approach in relevant biological and toxicological media. In general, PtNPs sizes measured using dynamic light scattering, field flow fractionation, single-particle inductively-coupled plasma-mass spectroscopy, transmission electron microscopy and atomic force microscopy, were all in good agreement when PtNP sizes were larger than the size detection limits of each analytical technique. Slight differences in sizes measured were attributable to differences in analytical techniques, measuring principles, NP shape and NP permeability. The thickness of the PVP layer increased (from 4.4 to 11.35 nm) with increases in NP size. The critical coagulation concentration of cit-PtNPs was independent of NP size, possibly due to differences in PtNPs surface charges as a function of NP size. PtNPs did not undergo significant dissolution in any media tested. PtNPs did not aggregate significantly in Dulbecco's modified Eagle's medium; but they formed aggregates in moderately hard water and in 30 ppt synthetic seawater, and aggregate size increased with increases in PtNPs concentration. Overall, this study describes a general model NP system (i.e., PtNPs) of different controlled NP sizes and coatings that is predictable, stable and useful to investigate the fate, behavior, uptake, and eco-toxicity of NPs in the environment.

© 2019 Elsevier Inc. All rights reserved.

1. Introduction

The global production of platinum group elements (PGE) has grown steadily since 1970, and the global production of platinum

^{*} Corresponding author at: Department of Environmental Health Sciences, University of South Carolina, 921 Assembly Street, Columbia, SC 29208, USA. E-mail address: mbaalous@mailbox.sc.edu (M. Baalousha).

(Pt) alone increased to 190 tons with an annual demand of 257 tons in 2016 [1]. The main use of Pt is in the catalytic convertors of cars, trucks, and buses, accounting for approximately 50% of Pt demand each year. Mandatory installation of catalytic convertors in motor vehicles reduced the emission of harmful exhaust emissions (e.g. carbon monoxide, nitrogen and sulfur oxides, hydrocarbons, aldehydes, and heavy metals etc.) [2,3], but it resulted in an increased release of PGE (i.e. Pt, Pd, Rh, Ru, Os and Ir) to the environment [4], and some studies demonstrated the release of Pt in the form of nanoparticles (NPs) [5,6]. The concentration of Pt in environmental samples, such as road dust, soil, surface water, sediments and plants has increased significantly in recent decades [7-11]. The concentration of Pt in aquatic ecosystems (0.4–10.8 ng-Pt·L⁻¹) is relatively low compared to their concentration in the immediate vicinity of roads (50 ng-Pt·g⁻¹ of road dust) [3]. Even higher Pt concentration (>300 $\mu g \cdot g^{-1}$) has been reported in Mexico city road dust [9]. Additionally, Pt complexes (e.g., cisplatin, carboplatin) are used for cancer treatment [12], and platinum nanoparticles (PtNPs) have shown promise in this use [13]. The majority of drugs containing Pt complexes are excreted in patients' urine (about 70%) and enter wastewater systems [4]. Treatment removal methods for these active compounds are lacking which contributes to environmental Pt contamination [4,14].

Several studies have reported Pt toxicity to aquatic organisms including water fleas (*Daphnia magna*, 3-weeks $LC_{50} = 520 \, \mu g \cdot L^{-1}$) [15], freshwater oligochaetes (*Variegatus lubriculus*, 96-h $LC_{50} = 0.4$ –30 mg· L^{-1}) [16], freshwater microalgae (*Pseudokirchneriella subcapitata*, 72-h $EC_{50} = 17 \, \text{mg·}L^{-1}$) [17], and marine bacteria (*Photobacterium phosphoreum*, $EC_{50} = 25 \, \mu g \cdot L^{-1}$) [18]. A recent study also reported reproductive toxicity of PtNPs to zebra fish after chronic exposure [19].

Currently little is known about the environmental behaviors of PtNPs such as aggregation and dissolution in environmental media. Understanding the nature of exposure and the physicochemical transformations of PtNPs during (eco)toxicology exposures is essential to interpret and quantify dose-response relationships. These transformations, which are likely to occur in (eco)toxicological media during acute to chronic exposure periods, have been investigated extensively for other NPs (e.g., AgNPs, AuNPs, CeO₂-NPs etc.) [20–22] but not for PtNPs. According to previous studies (with other NPs), aggregation and/or dissolution can significantly alter NP behavior (e.g., dosimetry, bioavailability, uptake, toxicity) and fate (e.g., pharmacokinetics and biodistribution) [23-25]. Therefore, the purpose of this study was to improve understanding of PtNPs environmental behaviors by (1) developing reproducible protocols for controlled synthesis of monodispersed PtNPs of five different sizes and two coatings (citrate and polyvinylpyrrolidone; PVP); (2) evaluating aggregation kinetics of PtNPs in the presence of monovalent (i.e., NaNO₃) and divalent electrolyte (i.e., Ca (NO₃)₂); and (3) measuring the colloidal stability (e.g., aggregation and dissolution) of cit- and PVP-coated PtNPs in three different media relevant to biological systems but differing in ionic strengths and compositions.

2. Methodology

2.1. Particle synthesis

Citrate- and polyvinylpyrrolidone-coated PtNPs (cit-PtNPs and PVP-PtNPs) of five different core sizes ranging from 5 to 75 nm (labelled as PtNPs A, B, C, D, and E) were synthesized by modifying the PtNPs synthesis protocol developed by Bigall et al. [29] as described below. Monodispersed PtNPs were synthesized to avoid confounding results due to NP polydispersity [26]. Citrate and PVP surface coatings were used as model surface coatings because they

are well-characterized, widely used in published studies, and they impart two mechanisms of NP stabilization (*e.g.*, electrostatic stabilization and steric stabilization, respectively) [27,28].

PtNPs A. Spherical cit-PtNP seed suspensions (8.7 nm diameter) were synthesized according to previously published synthesis protocols [29,30]. Briefly, 36 mL of 5 mM chloroplatinic acid hydrate (H₂PtCl₆, ≥99.9% pure, supplied by Sigma-Aldrich, St. Louis, USA) was added to 464 mL ultra-high pure water (UHPW, 18.2 MΩ·cm) at the boiling point in a 1000 mL Erlenmeyer flask. 50 µL of 1 M sodium hydroxide (NaOH, supplied by Sigma-Aldrich, St. Louis, USA) was then added to the solution to enhance production of monodispersed small PtNPs (<10 nm) [31]. After 1 min, 11 mL of 1% sodium citrate solution were added dropwise. After 30 s, 5.5 mL of a solution containing 0.08% sodium borohydride (NaBH₄, >98% pure, supplied by Alfa Aesar, Ward Hill, USA) and 1% sodium citrate (Na₃C₆H₅O₇, supplied by VWR International, West Chester. USA) were added quickly to the boiling solution. After 10 min of boiling, the product was left to cool to room temperature. All reactions took place under vigorous stirring (i.e., 700 rpm).

PtNPs B. 10 mL PtNP A suspension were diluted in 290 mL UHPW, to which 450 μ L of 0.4 M H₂PtCl₆ were added under constant stirring (700 rpm). 5 mL of 1% sodium citrate and 1.25% L-ascorbic acid (aqueous) were added dropwise (1 drop per 3 s) to the PtNP and H₂PtCl₆ mixture. The temperature was slowly raised (~10 °C per minute) to boiling under vigorous stirring (*i.e.*, 700 rpm) and then poised at the boiling point (100 °C) for 30 min. The resulting suspension was left to cool to room temperature.

PtNPs C, D, and E. Larger PtNPs (PtNPs C, D, and E) were synthesized by diluting different volumes (40, 10, and 2.5 mL) of the PtNPs B in 260, 290, and 298 mL UHPW, respectively. 450 μL of 0.4 M $H_2 PtCl_6$ solution were added to the diluted suspensions under vigorous stirring (700 rpm). 5 mL solution containing 1% sodium citrate and 1.25% L-ascorbic acid were then added dropwise. The temperature was raised slowly to boiling, as above, under vigorous stirring for 30 min and left to cool to room temperature.

Purification of PtNPs. All synthesized cit-PtNP suspensions were washed three times by ultrafiltration to remove excess reagents. 300 mL cit-PtNP suspension were reduced to 150 mL by ultrafiltration over 3 kDa regenerated cellulose membrane using an Amicon® stirred-cell ultrafiltration unit (EMD Millipore Corporation, MA, USA) under 15 psi pressure (nitrogen). The PtNP suspension was replenished with 150 mL solution of 1% sodium citrate.

PVP-PtNPs were obtained by a ligand exchange approach using cit-PtNPs as precursors [20]. Briefly, 300 mL cit-PtNPs of different sizes (PtNPs A, B, C, D, and E) were converted into PVP-PtNPs by adding 1, 0.85, 0.48, 0.20, and 0.12 mL of 7.7 mM PVP solution, respectively, under vigorous stirring (700 rpm) for at least 1 h. The PVP amount selected was that required to obtain full surface coverage of PtNPs by PVP molecules and also sufficient to impart full steric stabilization [28], assuming that PtNPs are spherical and that 8 PVP molecules/nm² are required to fully cover a PtNP surface.

Concentrations of synthesized cit- and PVP-PtNPs were measured using a NexION 350D inductively coupled plasma-mass spectrometer (ICP-MS). 1 mL aliquots of each PtNP suspension were digested using 1 mL freshly-prepared aqua regia at room temperature for 24 h. Aqua regia was prepared by mixing 1 mL hydrochloric acid (trace metal grade, 35–38%, Fisher scientific, MA, USA) and 3 mL nitric acid (trace metal grade, 68–70%, Fisher scientific, MA, USA) in acid cleaned glassware. The digested PtNP solutions were diluted at least 3000 folds prior to analysis by ICP-MS, and all samples were measured in triplicate.

2.2. Particle characterizations

The z-average diffusion coefficient and electrophoretic mobility (EPM) of the synthesized PtNPs were measured by dynamic light scattering (DLS) and laser Doppler electrophoresis using a Zetasizer Nano-ZS instrument (Malvern Instruments Ltd., MA, USA). All measurements were performed at 25 °C after a 2-min temperature equilibration. The z-average hydrodynamic diameter (d_{DLS}) was calculated from the diffusion coefficient using Stokes-Einstein equation. The zeta potential (ζ) was calculated from the electrophoretic mobility using Smoluchowski's assumption [32]. The d_{DLS} and ζ were reported as the mean and standard deviation of five and ten replicates, respectively.

Samples for transmission electron microscopy (TEM) analysis were prepared by depositing a drop of the washed PVP-PtNP suspensions on a copper grid (300 mesh) coated with a thin film of continuous carbon (Agar Scientific, Stansted, Essex, UK) at room temperature. After 20 min, the grids were washed thoroughly with UHPW to avoid salt crystallization and NP aggregation artefacts [21]. The grids were then left to dry overnight under ambient conditions in a covered petri dish to avoid atmospheric particle deposition. Samples were analyzed in a LaB₆ Jeol 2100 TEM (Joel USA Inc., MA, USA), operated at 200 keV and equipped with a Jeol EX-230 Silicon Drift Detector (SDD; manufactured by Joel USA Inc., MA, USA) with a 60 cm² window of acquisition for Energy Dispersive X-ray Spectroscopy (EDS) analysis of elements. Micrographs were acquired at different magnifications, ranging from 500X to 400,000X, to gather information about the average size, morphology, and degree of aggregation (if any) of nanoparticles on the grid. At least 150 NPs were analyzed from each sample to construct a representative particle-size distribution using the Gatan Digital Micrograph software package (GMS 3) [33].

Samples for atomic force microscopy (AFM) analysis were prepared by depositing a drop of PVP-PtNPs suspension in the presence of 2 mM calcium on a freshly cleaved mica substrate for 20 min. That was followed by thorough rinsing with UHPW to avoid salt crystallization and NP aggregation [34]. The mica sheets were then left to dry overnight under ambient conditions in a covered petri dish. AFM analysis was performed on a Cypher ES™ AFM microscope (Asylum Research, CA, USA). Images were recorded in ACAirTopography mode using a silicon cantilever (Asylum Research, CA, USA) with a spring constant of 26 (11–54) N m⁻¹. The scanning rates were optimized to acquire a stable and clear image without damaging the AFM tip or detaching the NPs from the AFM substrate [21], usually 0.25–1 Hz scan rate. At least five different areas on each substrate were analyzed, yielding a minimum of five images (image size = $5 \times 5 \mu m$) from each area and producing at least 25 images for each substrate. For each sample, at least 150 height measurements were performed which is sufficient to produce a representative and robust particle size distribution [35]. This distribution was used to calculate mean core diameter (d_{AFM}) of each PtNP collection.

Flow-Field flow fractionation (FIFFF) analysis was performed using a Wyatt Ecilipse® DualTec™ asymmetrical FIFFF instrument (Wyatt Technology Corporation, CA, USA). A 1-kDa OMEGA™ Polyethersulfone membrane (Pall Corporation, NY, USA) was used as an accumulation wall. The carrier phase was 10 mM NaNO₃ (pH 7). The channel flow and cross flow were maintained at 1 mL min $^{-1}$. The injection volume was 0.25 mL (particle concentration 1 mg L $^{-1}$), and the focus time was 5 min. Four polystyrene Nanosphere™ size standards (22 ± 2, 41 ± 4, 81 ± 3, and 152 ± 5 nm manufactured by Thermo scientific, CA, USA) were used to calibrate the effective channel thickness for particle size conversion. All particles were detected with a UV detector at 370 nm. Hydrodynamic diameter (d_{FIFFF}) of PtNPs was calculated

using a calibration curve for size and retention time established using the polystyrene size standards.

Particle number concentration and number size distribution were measured by single particle ICP-MS (sp-ICP-MS). All sp-ICP-MS [36–40] data were acquired with a NexION™ 350D ICP-MS (PerkinElmer Inc., MA, USA) operating in a single particle mode with the Syngistix Nano Application Module. A standard introduction system consisting of a Meinhard glass concentric nebulizer, a glass cyclonic spray chamber, and a 2 mm ID quartz injector was used. The sample uptake rate was 0.28 mL/min. Data were acquired at an RF power of 1600 W, a 50 µs dwell time, a 0 µs settling time, and a 60 s acquisition time. The transport efficiency for PtNPs C, D, and E were 10.3%, 10.0%, and 11.1%, respectively. NIST™ Au standard reference material (actual TEM size of 56 nm; reference material 8013 manufactured by U.S. National Institute of Standards and Technology, MD, USA) was used to determine the transport efficiency. A rinse cycle consisting of 1 min with 1% aqua regia, and 1 min with UHPW was performed after each sample run to ensure cleansing of the sample introduction system between samples. All PtNPs suspensions (A-E) were measured in triplicate at 5 different concentrations (e.g., 100, 200, 400, 600, and 800 ng·L⁻¹) with results reported as the mean ± standard deviation of 3 replicates. (d_{sp-ICP-MS}). The NIST Au standard reference material was measured after each set as a QA/QC check.

2.3. Aggregation kinetics

Using DLS, cit-PtNPs A-E aggregation kinetics were measured at pH 7 in duplicate in different electrolyte concentrations (0–70 mM NaNO₃, and 0–10 mM Ca(NO₃)₂) by monitoring the growth of NP z-average hydrodynamic diameters (d_{DLS}) over time immediately after mixing (within 10 s) with electrolyte (NaNO₃, and Ca(NO₃)₂) and at repeated intervals of 15 s for 10 min at 25 \pm 0.5 °C. The count rate during DLS measurement increased with time in the range of 30–200 kcps due to increasing aggregate sizes. The aggregation rate constant (k) is proportional to the d_{DLS} rate of change (i.e., the slope of the hydrodynamic diameter as a function of time, Eq. (1)) [41], which was determined by fitting a linear correlation function to the experimental data collected during early stage aggregation.

$$k = \frac{1}{2Nd_2} \frac{d_r}{d_r} \tag{1}$$

where N is the initial NP concentration, d_0 is the initial NP diameter, and o is the optical factor.

The attachment efficiency ($\alpha = \frac{1}{W}$) was determined according to Eq. (2).

$$\alpha = \frac{1}{W} = \frac{K_{slow}}{K_{fast}} \tag{2}$$

where W is the colloidal stability ratio, and k_{slow} and k_{fast} are the slow and fast aggregation rates representing the aggregation rates under the reaction (RLA) and diffusion (DLA) limited aggregation regimes, respectively. The DLA occurs at counter-ion concentrations above the critical coagulation concentration (CCC); whereas the RLA occurs at counter-ion concentrations below the CCC. The CCC represents the minimum counter-ion concentration required to completely destabilize the NP suspension [42]. The attachment efficiencies under RLA and DLA regimes were fitted by linear functions, with their intersection yielding the respective CCC reported.

2.4. Colloidal stability of PtNPs in (eco)toxicological media

The colloidal stability of citrate- and PVP-PtNPs E was investigated as a function of NP concentration (*e.g.*, 20, 200, 2000 μg·L⁻¹)

in three (eco)toxicological media including Moderately hard water (MHW), 30 ppt synthetic seawater (SW), and Dulbecco's modified Eagle's medium (DMEM). MHW media is widely used for acute and/or chronic toxicity tests with *Daphnia magna* [43] and *Lymnaea stagnalis* [44]. 30 ppt SW is common and recommended for toxicity tests with many marine organisms (e.g., *Amphiascus tenuiremis* [45]), and DMEM is typically used as a cell/cytotoxicity culture medium [46]. MHW was prepared according to US environmental protection agency (USEPA) guidelines [47]. Crystal Seas™ bioassay grade synthetic seawater was purchased from Instant Ocean® (Marine Enterprises International, Baltimore, MD, USA). DMEM was purchased from American Type Culture Collection (ATCC, Manassas, VA, USA). The chemical composition of MHW, synthetic seawater, and DMEM is given in Tables S4–6.

PtNPs E were incubated with the (eco)toxicological media in high density polyethylene (HDPE) sterile plastic vials (Fisher Scientific, MA, USA) under static conditions in the absence of light [20]. All vials were washed with 10% nitric acid for at least 24 h and rinsed in UHPW for another 24 h prior to the experiment. PtNP hydrodynamic diameter and zeta potential were measured by DLS and laser Doppler electrophoresis. Size distribution and number concentration were measured by sp-ICP-MS, and pH was measured by Mettler Toledo F20-Kit FiveEasy™ Benchtop pH meter (Hogentogler & co. Inc., Columbia, MD, USA). All parameters were measured immediately after mixing and 24 h post mixing for the different media at different NP concentrations. For the colloidal stability test, sp-ICP-MS analysis was performed following the same procedure described above (see particle characterizations section). However, the instrument rinsing time between samples was increased to 5 min (1 min with 1% nitric acid, 2 min with 1% aqua regia, followed by 2 min with UHPW) to ensure that all salts, organic matter, and metals were removed from the system to eliminate cross- contamination, nebulizer fouling, or changes in NP transport efficiency.

3. Results and discussions

3.1. Particle synthesis

A facile seed-mediated growth synthesis protocol was successfully adapted [29] to produce spherical cit-PtNPs (A-E) of five different sizes, ranging from 9.2 to 72.5 nm. All five cit-PtNP suspensions showed a pH of 7.0 ± 0.1 , were black in color immediately after preparation, and were stable over several months when stored at 4 °C in the dark. Initially, the seed (PtNP A) was produced by reducing the Pt precursor (H₂PtCl₆) using a strong reducing agent (NaBH₄, redox potential -1.37 to 0.4 V) [48]. Larger cit-PtNPs (cit-PtNP B) were produced via a "seedmediated growth" process using cit-PtNP A as a nucleus to which a Pt precursor was added in the presence of a weak reducing agent (i.e., 1-ascorbic acid, redox potential -0.55 to 0.35 V) [49]. The weak reducing agent reduces Pt ions to metallic Pt without inducing a new nucleation event. Thus metallic Pt atoms precipitate on the surface of already existing nuclei resulting in particle growth [48]. Larger cit-PtNPs (cit-PtNP C, D, and E) were synthesized following the same seed-mediated growth process discussed above but using cit-PtNP B as the seed nucleus. Different cit-PtNP sizes were produced by varying initial seed concentrations. A higher seed concentration, and thus a higher seed number, provided a higher number of sites for the precipitation of metallic Pt atoms resulting in the formation of smaller cit-PtNP sizes, and vice versa. Subsequently, PVP-PtNPs A-E were obtained from their corresponding cit-PtNPs collections by ligand exchange.

3.2. Particle characterizations

The physicochemical properties of the synthesized PtNPs were measured using a multi method approach [50,51]. Representative TEM and AFM micrographs of PVP-PtNPs A-E are presented in Fig. 1a-e and Fig. S1a-e, respectively. All TEM and AFM micrographs show randomly-distributed NPs, without agglomerates, indicating robust sample preparation and desired dispersion of PVP-PtNPs [52]. TEM images (Fig. 1) show that synthesized PVP-PtNPs (A-E) are spherical. High resolution TEM images of PtNPs C, D, and E (Fig. S2) illustrate the formation of a thick PVP coating (2.7–5.6 nm thick) on the surface of PtNPs. Such a PVP coating was not observed on the surface of PtNP A and B, possibly because the PVP coating thickness around PVP-PtNP A and B was not thick enough to be imaged by TEM. Elemental analysis (using EDS coupled with TEM) of the synthesized NPs confirmed that they were composed of Pt (Fig. S3).

Fig. 2 presents the PSD of PVP-PtNPs A-E obtained by TEM, AFM, sp-ICP-MS, DLS, and FIFFF. The size distributions measured by TEM, AFM, and FIFFF show that PtNPs A, B, D, and E exhibit a monomodal PSD, whereas PVP-PtNPs C exhibits a bimodal PSD. For PtNPs C, the size distribution measured by TEM shows that the main peak (77% of the total number of NPs) is centered at 19 nm and the minor peak of smaller particles (23% of the total number of NPs) is centered at 11-12 nm. The size of the smaller particles in PVP-PtNPs C corresponds to that of PVP-PtNPs B, indicating that some seed nuclei did not grow to larger particles possibly due to the limited concentration of added Pt precursor. The size distributions measured by sp-ICP-MS show that PVP-PtNPs A, B, and C have similar size distributions within the range $25 \pm 2-32 \pm 3$ nm, and that PVP-PtNPs D and E are characterized by a monomodal PSD. The PSD of PVP-PtNPs A, B, and C are characterized by a half Gaussian distribution, possibly due to the detection of large PVP-PtNPs only (i.e., PtNPs > the lower size detection limit of ~20 nm) [53]. DLS measured size distributions suggest that all PVP-PtNPs exhibited monomodal PSDs because the lower size resolution of DLS cannot resolve such small differences in NP size distribution compared with the higher resolution of TEM, AFM, and FIFFF.

The mean sizes of PVP-PtNPs A-E, as measured by five different techniques (Table 1), are different and generally follow the order $d_{AFM} < \sim d_{TEM} < d_{sp-ICP-MS} < d_{FIFFFF} < d_{DLS}$ with few exceptions. These exceptions likely can be attributed to inherent limitations of each analytical technique. For example, $d_{sp-ICP-MS} > d_{FIFFF}$ for PVP-PtNPs A and B. This can be explained by the lower size detection limit of sp-ICP-MS and subsequent overestimation of PVP-PtNPs A and B mean sizes by sp-ICP-MS. The discrepancies in measured mean sizes obtained by different techniques can be attributed to differences in (i) measurement principles, (ii) the obtained measurand, (iii) PSD weighting, and (iv) NP structure [35,51].

Whereas TEM, AFM, and sp-ICP-MS all measure particle core size, DLS, and FIFFF measure NP hydrodynamic diameter (*i.e.*, core size + diffuse layer). Thus, the NP sizes measured by DLS and FIFFF are generally larger than those measured by TEM, AFM, and sp-ICP-MS. TEM measures a projected surface area from which an equivalent circular diameter can be calculated assuming spherical particle shape. AFM measures NP height, which is typically assumed equal to particle diameter and that all particles are spheres [54,55]. Both TEM and AFM techniques give number-based PSD and number average size. The mean sizes measured here by TEM and AFM were in good agreement (within $\pm 10\%$; $d_{AFM}/d_{TEM} = 0.92-1.08$) for all five PtNPs (Table 1).

sp-ICP-MS measures NP number-based core size. For the larger PtNPs (D and E), the mean sizes measured by sp-ICP-MS are in good agreement with those measured by TEM and AFM because they are larger than the lower size detection limit by sp-ICP-MS (*i.e.*, 20 nm for PtNPs) [53]. The PSDs of PtNPs suspensions A, B,

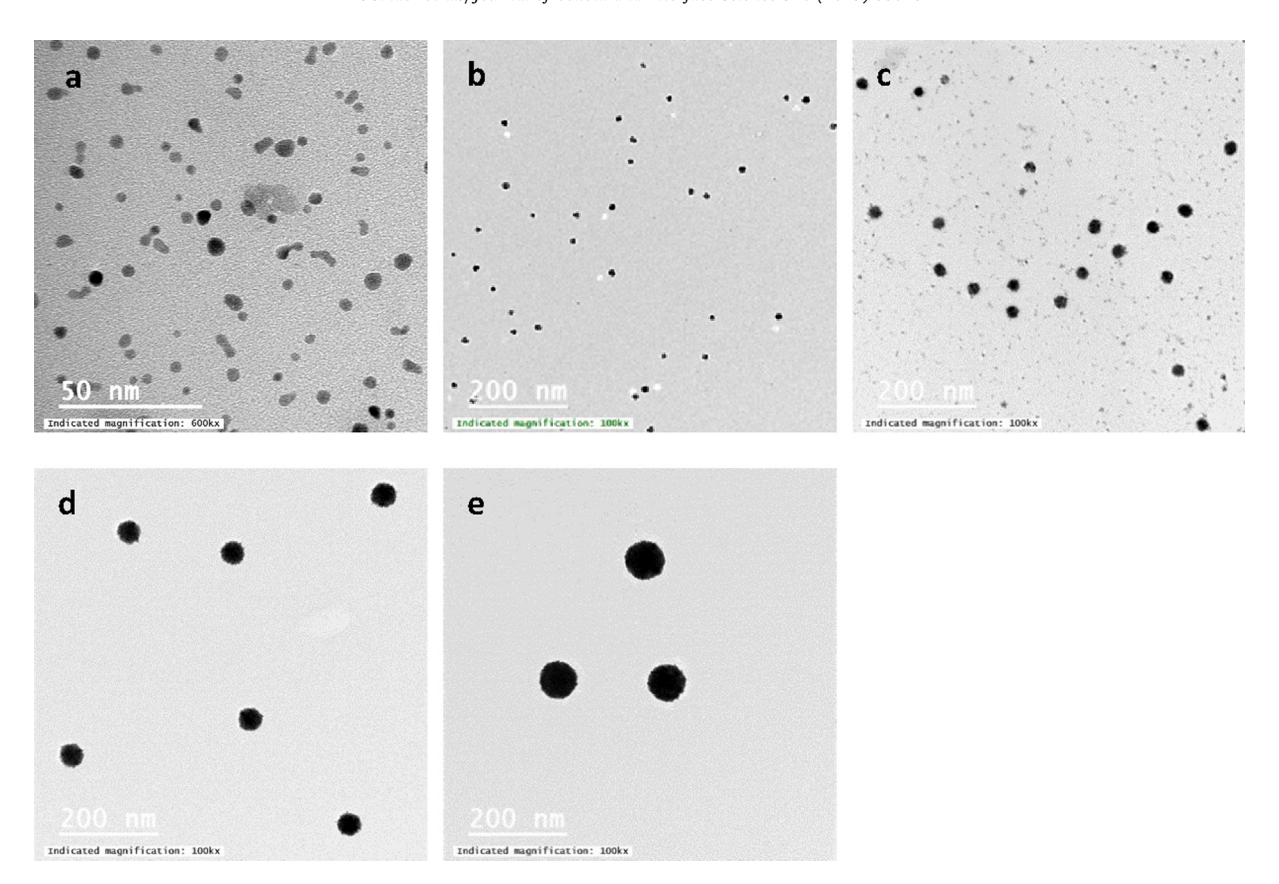


Fig. 1. Typical transmission electron microscopy (TEM) micrographs of synthesized PVP-PtNPs for (a-e) PVP-PtNPs A, B, C, D, and E, respectively.

and, C obtained by sp-ICP-MS are monomodal but present curtailed log-normal size distributions. This is because the smaller particles detected by TEM, AFM and FIFFF are below the size detection limit of sp-ICP-MS. Hence, the d_{sp-ICP-MS} of PtNPs A, B, and C are larger than those measured by TEM.

DLS and FIFFF measure NP diffusion coefficients, from which NP equivalent hydrodynamic diameter can be calculated using the Stokes-Einstein equation, assuming NPs are hard spheres [56]. D_{DLS}/d_{FIFFF} varied within a range of 0.98–1.39 for PVP-PtNPs A-D and was 0.89 for PVP-PtNPs E. The higher hydrodynamic diameter obtained by DLS compared to FIFFF is because DLS measures intensity-based PSD whereas FIFFF-coupled to UV-vis measures mass-based PSD. The larger hydrodynamic diameter of PVP-PtNPs E measured by FIFFF can be attributed to NP-membrane interaction in the FIFFF channel resulting in retardation of NP elution as indicated by a tailing of the FIFFF PSD of PVP-PtNP E (Fig. 2e).

For citrate-PtNPs B, D, and E, the d_{DLS} decreased with the addition of 20 mM NaNO $_3$ compared to d_{DLS} in UHPW (Table 1). This was likely due to shrinkage of the diffuse double layer after addition of NaNO $_3$ [57]. As a result, d_{DLS} of cit-PtNPs measured in 20 mM NaNO $_3$ were in closer agreement to those measured by TEM than to those measured in UHPW. NaNO $_3$ addition provides a useful way to measure NPs core size via DLS by increasing the NP suspension ionic strength to shrink the diffuse layer without inducing NP aggregation. For PtNP A and C, the d_{DLS} did not change with the addition of 20 mM NaNO $_3$ compared to d_{DLS} in UHPW, which might be attributed to the higher polydispersity of PtNP A and C (σ/d_{TEM} > 0.13) compared to PtNP B, D and E (σ/d_{TEM} < 0.09).

For the same PtNP, the d_{DLS} of PVP-PtNPs were larger than the corresponding d_{DLS} of cit-PtNPs by 9–23 nm, depending on the particle (Table 1). This is attributed to surface coating exchange and

the formation of a thick PVP coating (4.4–11.4 nm thick), and is in good agreement with TEM analysis (Fig. S2a–c) [58]. Moreover, d_{DLS}/d_{TEM} of cit-PtNPs range from 1.1 to 1.7 (Table 1), and those for PVP-PtNPs range from 1.3 to 2.9. This variability between small-ion (citrate) stabilized PtNPs and large polymer (PVP) stabilized PtNPs is mainly due to structural differences between PtNPs. The higher ratios (d_{DLS}/d_{TEM}) of PVP-PtNPs are due to polymer softness/permeability and because these particles do not satisfy the assumptions of the Stokes-Einstein relationship for hard spherical NPs. Based on our data, citrate-coated NPs may be considered hard spheres whereas PVP coated NPs behave as soft permeable particles which agrees with previous studies with different NPs [35,59].

The magnitude of ζ increase with increase in cit-PtNP size (Fig. S4) can be attributed to (1) increases in surface Pt oxidation state (e.g., Pt⁰ to Pt⁺² and/or Pt⁴⁺) with decreases in PtNP size, and/or (2) insufficient/partial citrate coating on smaller PtNP surfaces (i.e., variability in the amount of citrate per unit surface area). The concentration of citrate molecules is the same for all PtNPs. The specific surface area of PtNPs increases with decreases in NP size. Thus the number of available citrate molecules per unit surface area decreases with decrease in PtNP size. The first mechanism can be ruled out because surface Pt oxidation state increases only for PtNPs < 6 nm [60], and all PtNPs used in this study were >10 nm. To evaluate the second mechanism, the zeta potential of PtNPs A was measured as a function of sodium citrate concentration (Fig. S5). The ζ of PtNPs A increased with increasing sodium citrate concentration which is indicative of an increased surface coating and corresponding surface charge as sodium citrate increased. Conversely, the decrease in magnitude of ζ with decreases in particle size can be attributed to insufficient coating of smaller PtNPs with citrate molecules due to correspondingly larger specific surface areas.

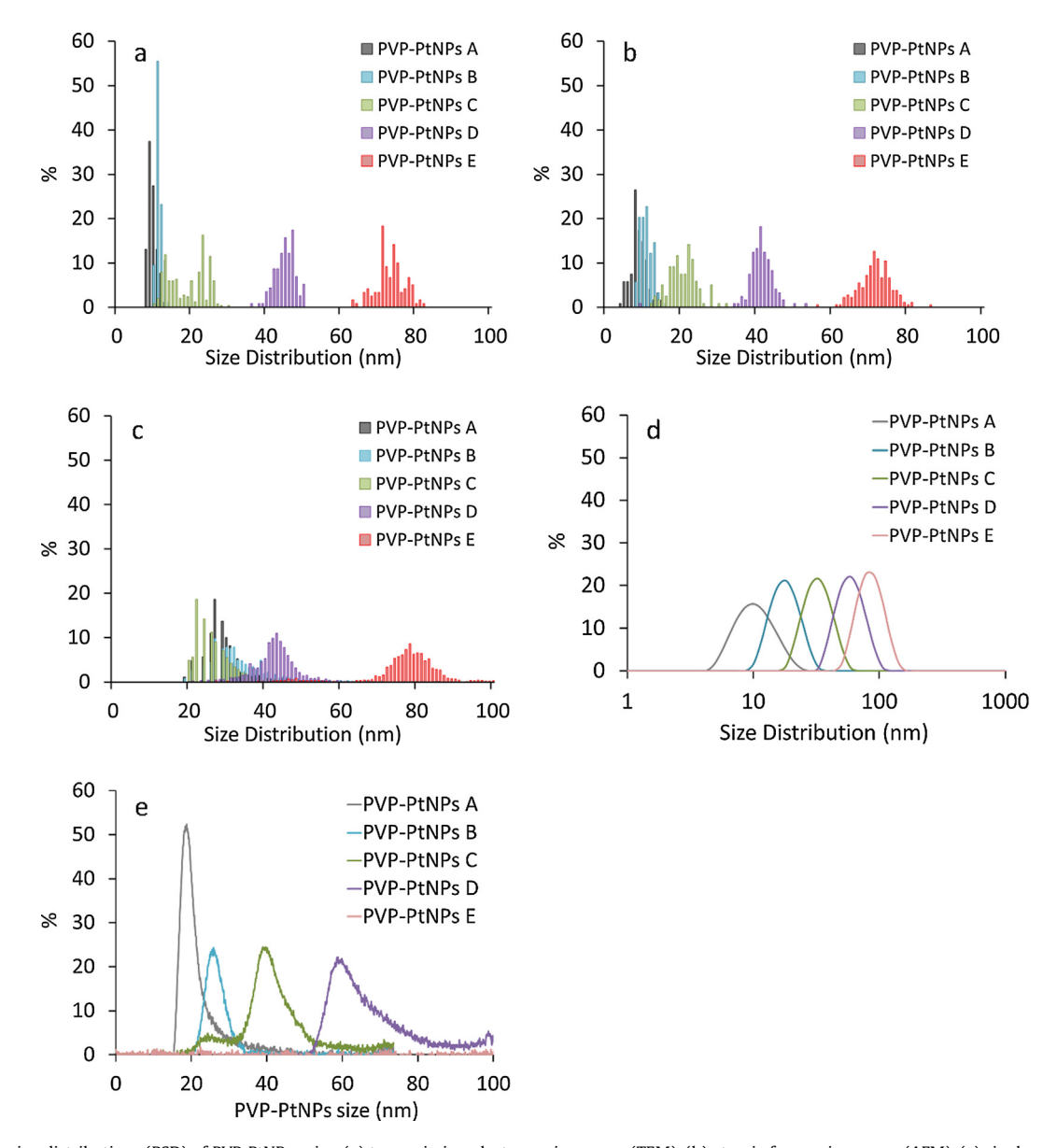


Fig. 2. Particle size distributions (PSD) of PVP-PtNPs using (a) transmission electron microscopy (TEM), (b) atomic force microscopy (AFM), (c) single particle inductively-coupled plasma mass spectroscopy (sp-ICP-MS), (d) dynamic light scattering (DLS), and (e) field flow fractionation (FFF) with UV-vis as a detector, cross flow and channel flow of 1 mL/min, and elution time of 60 min.

3.3. Aggregation behavior of cit-PtNPs

Increases in electrolyte concentrations (NaNO₃ and Ca(NO₃)₂) lead to a corresponding increase in d_{DLS} as a function of time up to a certain cation concentration, above which the d_{DLS} does not change (Fig. S6). In the presence of NaNO3, cit-PtNPs A (9.2 nm) did not show any aggregation up to 50 mM NaNO3 as the counter ion concentration was insufficient to screen the cit-PtNP A surface charge. At higher NaNO₃ concentrations (55-59 mM), cit-PtNPs A aggregation rates slowly increased as the repulsion barrier decreased, as suggested by DLVO (Derjaguin, Landau, Verway, and Overbeek) theory (Fig. S6a). At a NaNO₃ concentration higher than 60 mM, attractive van der Waals forces dominate over electrostatic repulsive forces resulting in fast aggregation of cit-PtNPs A. Growth in z-average diameter as a function of time did not change with further increases in NaNO₃ concentration (up to 90 mM). Similar aggregation behavior was observed for cit-PtNPs B-E (Fig. S6b-e). In the presence of divalent electrolyte (Ca(NO₃)₂), aggregation of cit-PtNPs was observed at much lower concentration of Ca^{2+} (e.g., 0.5–2.5 mM) compared to Na^+ concentration (e.g., 55–60 mM). Ca^{2+} ions are more efficient in screening the surface charge of cit-PtNPs compared to Na^+ (Fig. S6f–j). Additionally, Ca^{2+} ions can interact specifically with the carboxyl groups of citrate molecules adsorbed onto the surfaces of PtNPs [61].

The attachment efficiency of cit-PtNPs as a function of NaNO₃ (Fig. S7a-f) and Ca(NO₃)₂ (Fig. S7f-j) shows two different aggregation regimes, that is RLA and DLA, typical of DLVO type aggregation behavior. The RLA regime for cit-PtNP occurs within a narrow NaNO₃ and Ca(NO₃)₂ concentration range (ca. 53-65 and 1-3 mM for NaNO₃ and Ca(NO₃)₂, respectively), and the CCC values vary within a narrow counter ion concentration range for all cit-PtNP sizes. The CCC values in the presence of NaNO₃ and Ca(NO₃)₂ are presented in Table 2. The lower CCC values in the presence of Ca²⁺ compared to those measured in the presence of Na⁺ is in good agreement with the Schulze-Hardy rule (*i.e.*, the CCC is inversely proportional to counter ion valency) and with previous studies using citrate-coated silver nanoparticles [61,62].

Table 1Summary of PtNPs sizes measured by different sizing techniques. The reported sizes are for PVP-PtNPs, except where it is mentioned otherwise.

Method/measured or calculated parameter	Size of PtNPs suspensions (nm)				
	PtNPs A	PtNPs B	PtNPs C	PtNPs D	PtNPs E
AFM, $d_{AFM} \pm \sigma_d$	8.5 ± 1.2	10.3 ± 1.3	20 ± 4.77	40.5 ± 4.1	70.8 ± 4.2
TEM, $d_{TEM} \pm \sigma_d (d_{TEM}/\sigma_d)$	9.2 ± 1.2 (0.13)	$10.9 \pm 0.8 \; (0.09)$	18.5 ± 5.0 (0.27)	44.5 ± 2.7 (0.06)	$72.5 \pm 3.9 (0.05)$
sp-ICP-MS, dsp-ICP.MS $\pm \sigma_{d}$	26.3 ± 1.5	32.4 ± 2.5	24.7 ± 1.6	42.9 ± 0.8	77.1 ± 0.8
FIFFF, $d_{FFF} \pm \sigma_d$	19.3 ± 1.5	25.6 ± 2.7	36.7 ± 3.5	59.6 ± 5.2	105.4 ± 4.1
DLS, $d_{DLS} \pm \sigma_d$ (PDI)	18.9 ± 0.3 (0.36)	$31.4 \pm 0.8 (0.19)$	$51 \pm 0.7 (0.20)$	$74.7 \pm 0.2 (0.03)$	$93.4 \pm 1 \ (0.10)$
DLS (cit-PtNPs in UHPW), $d_{DLS} \pm \sigma_d$	10.0 ± 0.3	17.0 ± 0.3	31.6 ± 0.2	59.3 ± 0.3	83.5 ± 0.3
DLS (cit-PtNPs in 20 mM NaNO ₃), $d_{DLS} \pm \sigma_d$	10.1 ± 1.9	14.0 ± 0.6	32.6 ± 1.3	52.8 ± 0.7	70.7 ± 0.9
d _{DLS-PVP} - d _{DLS-cit-20 mM NaNO3}	8.8	17.4	18.4	21.9	22.7
PVP thickness	4.4	8.7	9.2	11	11.4
d_{AFM}/d_{TEM}	0.9	1	1.1	0.9	1
$d_{\text{sp-ICP-MS}}/d_{\text{TEM}}$	2.9	3	1.3	1	1.1
d_{DLS}/d_{FIFFF}	1	1.2	1.4	1.3	0.9

 $d_{\mbox{\scriptsize AFM}}\mbox{:}$ nanoparticle height measured by atomic force microscopy (AFM).

d_{TEM}: nanoparticle equivalent circular diameter measured by transmission electron microscopy (TEM).

d_{TEM}: nanoparticle equivalent spherical diameter measured by single particle-inductively coupled plasma-mass spectroscopy (sp-ICP-MS).

d_{FIFFF}: nanoparticle equivalent hydrodynamic diameter measured by flow-field flow fractionation (FIFFF).

d_{DLS}: nanoparticle equivalent hydrodynamic diameter measured by dynamic light scattering (DLS).

Table 2Critical coagulation concentration (CCC) of cit-PtNPs in presence of monovalent (NaNO₃) and divalent (Ca(NO₃)₂) electrolytes.

	CCC in NaNO ₃ (mM)	CCC in Ca(NO ₃) ₂ (mM)
cit-PtNPs A	63.6	1.1
cit-PtNPs B	65.2	2.7
cit-PtNPs C	53.6	2.6
cit-PtNPs D	61.7	1.5
cit-PtNPs E	54.2	1.5

No correlation was observed between CCC and cit-PtNP size (Table 2) for NaNO₃, or Ca(NO₃)₂. This is likely due to the increase in ζ magnitude with increasing cit-PtNP size (Fig. S4). There are currently contradictory data regarding the dependence of CCC on NPs size. Studies have reported a decrease in CCC with decreases in NPs size (e.g., hematite NPs [63], TiO₂-NPs [64]), an increase in CCC with decreases in NPs size (e.g. AgNPs [28], CdSe-NPs [65]), and independence of CCC relative to NPs size (e.g. AuNPs [66]). These contradictory results can be rationalized by taking into account the variability among NPs surface charges [28]. Negative correlation between CCC and NP size was observed for NPs characterized by a narrow range of ζ (ca. -33 ± 3 to -35 ± 5 for CdSe-NPs [65]), whereas positive correlation between CCC and NP size, or a size independence for CCC, were observed for NPs characterized by variable ζ [63,64,66].

Maximum cit-PtNPs aggregate sizes -- measured after 10 min in electrolyte concentrations (*e.g.*, 70 mM NaNO₃ and 10 mM Ca (NO₃)₂) greater than the CCC -- decreased with increases in cit-PtNPs initial hydrodynamic diameters (Fig. S8). Under these experimental conditions, the electrolyte concentration is sufficient to fully screen cit-PtNPs surface charge and dictate cit-PtNPs aggregation based on their diffusion [67]. With mass concentration held constant, smaller cit-PtNPs have a higher NPs number resulting in a higher collision probability and a subsequently larger mean aggregate size. Thus, under the same mass concentration and under diffusion limited aggregation conditions, smaller PtNPs form larger aggregates than larger PtNPs. Additionally, the maximum aggregate size of cit-PtNPs was larger in the presence of Ca²⁺ compared to Na⁺ (Fig. S8) and likely caused by cit-PtNPs aggregation enhancement via bridging mechanisms in the presence of Ca²⁺ [62].

3.4. The concentration-dependent behavior of PtNPs in toxicological media $\,$

The concentration-dependent colloidal stability (e.g. dissolution, aggregation) of cit- and PVP-PtNPs E was evaluated by mon-

itoring the change in d_{DLS} , ζ , number particle size distribution, and number particle concentration for PtNPs E (d_{TEM} = 72.5 ± 3.9 - nm) over 24 h in the three media (*i.e.*, MHW, SW, and DMEM). The pH of the PtNPs in DMEM, MHW, and SW media was 7.3 ± 0.1, 8.0 ± 0.1, and 8.1 ± 0.1, respectively.

The d_{DLS}, and ζ were monitored by DLS at an initial PtNPs concentration of 2000 $\mu g\ L^{-1}.$ The d_{DLS} of cit- and PVP-PtNPs in UHPW (control) were 89.5 ± 1.5 and 88.6 ± 1.9 nm, respectively (Fig. 3a and b). The d_{DLS} of cit- and PVP-PtNPs E increased slightly but significantly (two tailed t-test, p < 0.05) immediately after mixing with DMEM to 104.7 ± 3.9 and 105.4 ± 2.1 , respectively, compared to the UHPW control (Fig. 3a and b). This increase in the NP d_{DLS} might be attributed to sorption of organic compounds from the media [68,69] and/or the lower viscosity of DMEM media (0.94 mPa·s) compared to UHPW (1 mPa·s) [70]. The larger PtNPs hydrodynamic diameter in the DMEM media was likely due to the inverse correlation between size and viscosity (Stokes-Einstein relationship). The absolute ζ values of cit- and PVP-PtNPs E decreased from 48.3 ± 7.5 and 17.3 ± 1.5 mV in UHPW to 11.2 ± 9.2 and 6.9 ± 0.7 mV immediately after mixing with DMEM media (Fig. 3c and d). This indicates the replacement of citrate and PVP coatings by organic compounds in DMEM, and/or the screening of PtNPs surface charge by the abundant counter ions in DMEM. The d_{DLS} and ζ of cit- and PVP-PtNPs E did not change significantly (t-test, p > 0.05) in DMEM after 24 h compared to those measured at 0 h, indicating colloidal stability of both citand PVP-PtNPs in DMEM media despite a significant reduction in the ζ absolute values. DMEM media is rich with organic compounds (e.g., amino acids, vitamins, proteins) that are known to sorb onto NP surfaces to form a surface coating called "proteincorona" which may enhance NP colloidal stability via steric stabilization [68,69]. The z-average hydrodynamic diameter decreased after 24 h and may be attributed to the change in the nature and/or formation mechanisms of the protein-corona over time [71]. Formation of the protein-corona is dynamic in nature. Initially proteins with high concentrations and high association rate constants are adsorbed onto NP surfaces, and then they dissociate quickly to be replaced by proteins of lower concentration, slower exchange rates, and higher affinities [72]. Hence the thickness of the protein-corona may change over time due to changes in protein conformation following sorption onto NP surfaces.

The d_{DLS} of cit- and PVP-PtNPs E increased immediately after mixing with MHW and SW, and the d_{DLS} increased further after 24 h (Fig. 3a and b), indicating aggregation of cit- and PVP-PtNPs in both media. At 24 h, the d_{DLS} of cit- and PVP-PtNPs E was higher in SW (954.3 \pm 240.1 and 810.0 \pm 282.4, respectively) compared to

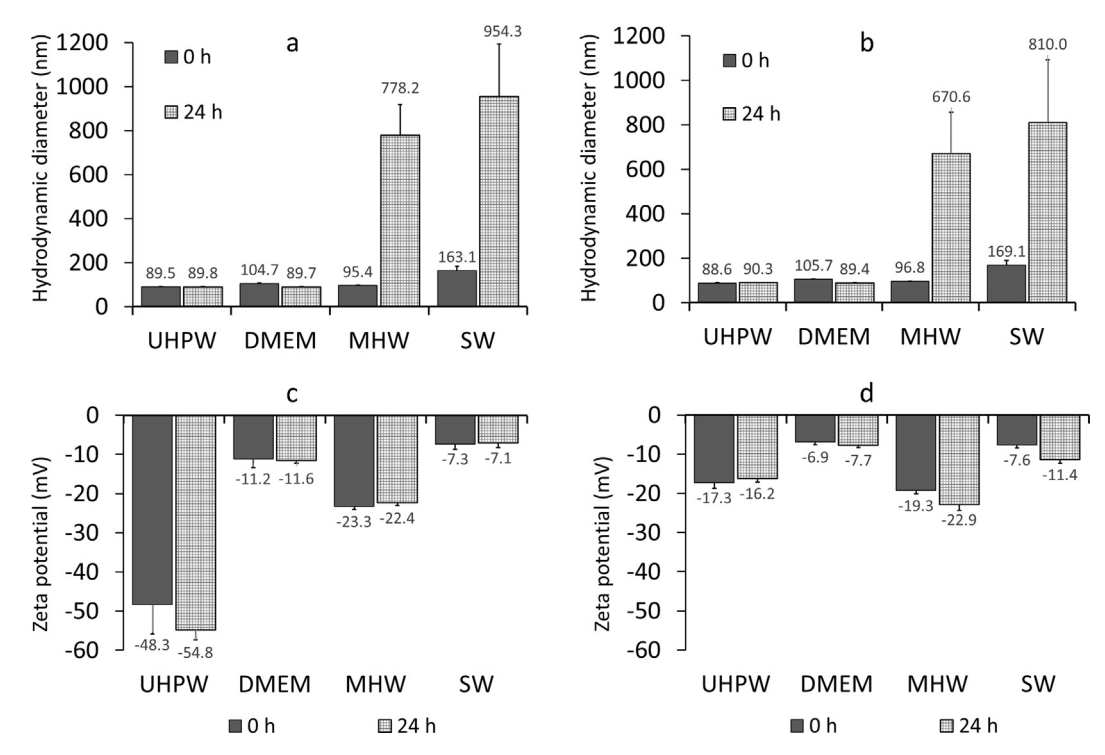


Fig. 3. (a and b) the equivalent hydrodynamic diameter ($d_{DLS.}$) and (b and c) the corresponding zeta-potential (ζ) of (a and c) cit-PtNPs and (b and b) PVP-PtNPs in ultra-high pure water (UHPW), Dulbecco's modified Eagle's medium (DMEM), Moderately hard water (MHW), and 30 ppt synthetic seawater (SW) media after 24 h of adding PtNPs in the corresponding media. PtNPs concentration in all suspensions are 2000 $ug \cdot L^{-1}$.

those measured in MHW (778.2 \pm 140.6 and 670.6 \pm 19.8, respectively), indicating higher aggregation in SW. The absolute ζ of citand PVP-PtNPs was lower in SW after 24 h (7.1 \pm 1.2, and 7.6 \pm 0.8 mV) compared to those measured in MHW (22.4 \pm 0.6 and 11.4 \pm 0.9 mV; Fig. 3c and d). The higher aggregation and surface charge screening in SW is due to the higher ionic strength of SW compared to MHW.

The cit-PtNPs and PVP-PtNPs did not undergo significant aggregation in DMEM despite the significant reduction in their absolute ζ 's, whereas they formed large aggregates in MHW despite the higher absolute ζ 's of PtNPs in MHW relative to DMEM. This indicates that PtNPs are charge-stabilized in MHW and sterically stabilized in DMEM. DMEM is rich with organic compounds (*e.g.*, amino acids, vitamins, proteins etc.) whereas MHW is prepared organic free. Hence, the organic molecule sorption onto the surface of PtNPs seems to enhance the colloidal stability of PtNPs in DMEM media via steric stabilization [68,69].

The concentration-dependent aggregation and dissolution of cit- and PVP-PtNPs E in DMEM, MHW and SW was further investigated by monitoring NP number concentration and number size distribution using sp-ICP-MS for initial NP concentrations between 20 and 2000 $\mu g \cdot L^{-1}$. The higher end of this concentration range coincides with that used to investigate PtNPs E aggregation by DLS. The lower end of the concentration range was selected as a more environmentally-relevant concentration [73].

At 2000 $\mu g \cdot L^{-1}$, PVP-PtNPs size distribution did not change in UHPW (Fig. 4c and S9a), increased slightly in DMEM (Fig. 4c and S9b), and increased significantly in MWH (Fig. 4c and S9c) and SW (Fig. 4c and S9d) over time. These results are in good agreement with the increase in PVP-PtNPs size measured by DLS (Fig. 3). However, the aggregate sizes measured by sp-ICP-MS are generally smaller compared to those measured by DLS due to differences in measured parameters and measurement principles as discussed above.

In DMEM, the size distribution of PVP- and cit-PtNPs did not change over time at $20~\mu g \cdot L^{-1}$ (Fig. 4a and S10a,d). It increased slightly with the appearance of a second peak at 90--100~nm at $200~\mu g \cdot L^{-1}$ (Fig. 4b and S10b,e) and $2000~\mu g \cdot L^{-1}$ PtNPs (Fig. 4c and S10c,f), concurrent with a decrease in the total particle number concentration (Table S5). In MHW and SW, cit- and PVP-PtNPs size distributions extended to larger sizes with mean sizes increasing with PtNPs concentrations (Figs. S11 and S12). Concurrently, primary NP number concentration (Figs. S11 and S12) and total particle number concentration (Table S5) decreased with increasing PtNPs concentrations.

For direct comparison, the % change in NP mean diameter and number concentration over 24 h as a function of NP concentration in the three media is presented in Fig. 5. At a given concentration, PtNPs mean sizes increased and the particle number concentrations decreased following the order SW > MHW > DMEM (Fig. 5b and d). For a given media, the % increase in PtNP mean size and the % decrease in PtNP total number concentration increased with increasing NP concentration. For DMEM, the PtNP mean diameter and number concentration did not change significantly over time (Fig. 5a and c). For MHW and SW, the particle diameter increased with increases in *initial* NP number concentration (Fig. 5a and c) concurrent with a decrease in *total* particle number concentration (Fig. 5b and d), thus indicating particle aggregation.

Despite PtNP aggregation in MHW and SW, a fraction of PtNPs remained as primary particles (Fig. 6 and S9–S12). The % of primary (unaggregated) particles increased with decreases in NP concentration (Fig. 6). This was due to a decrease in collision frequency, resulting in the formation of smaller aggregates and/or the lack of NP aggregation. These findings suggest that NP aggregation becomes less significant at lower concentrations, and that NPs may remain as primary particles for an extended period at environmentally relevant concentrations -- even in high ionic strength media such as MHW and SW. This is in good agreement with the

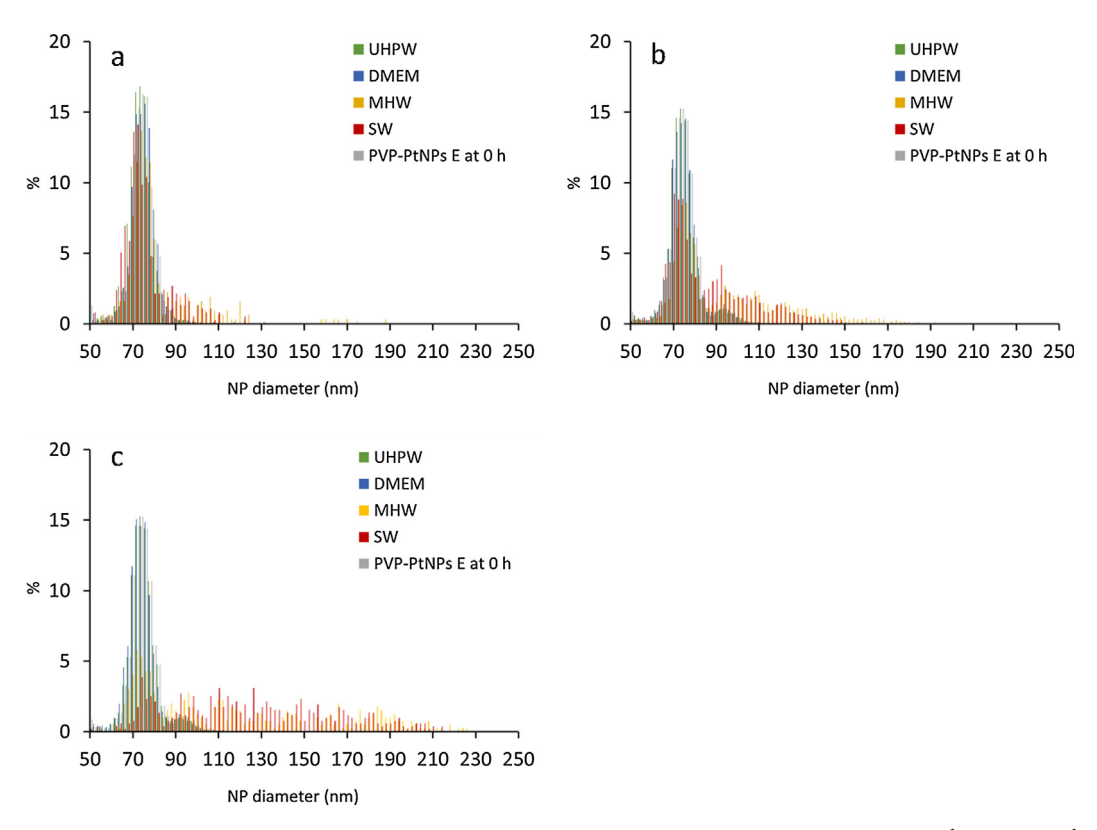


Fig. 4. Size distribution of PVP-PtNPs E after 24 h of adding the NPs to different media at initial exposure concentration of (a) 20 µg·L⁻¹, (b) 200 µg·L⁻¹, and (c) 2000 µg·L⁻¹

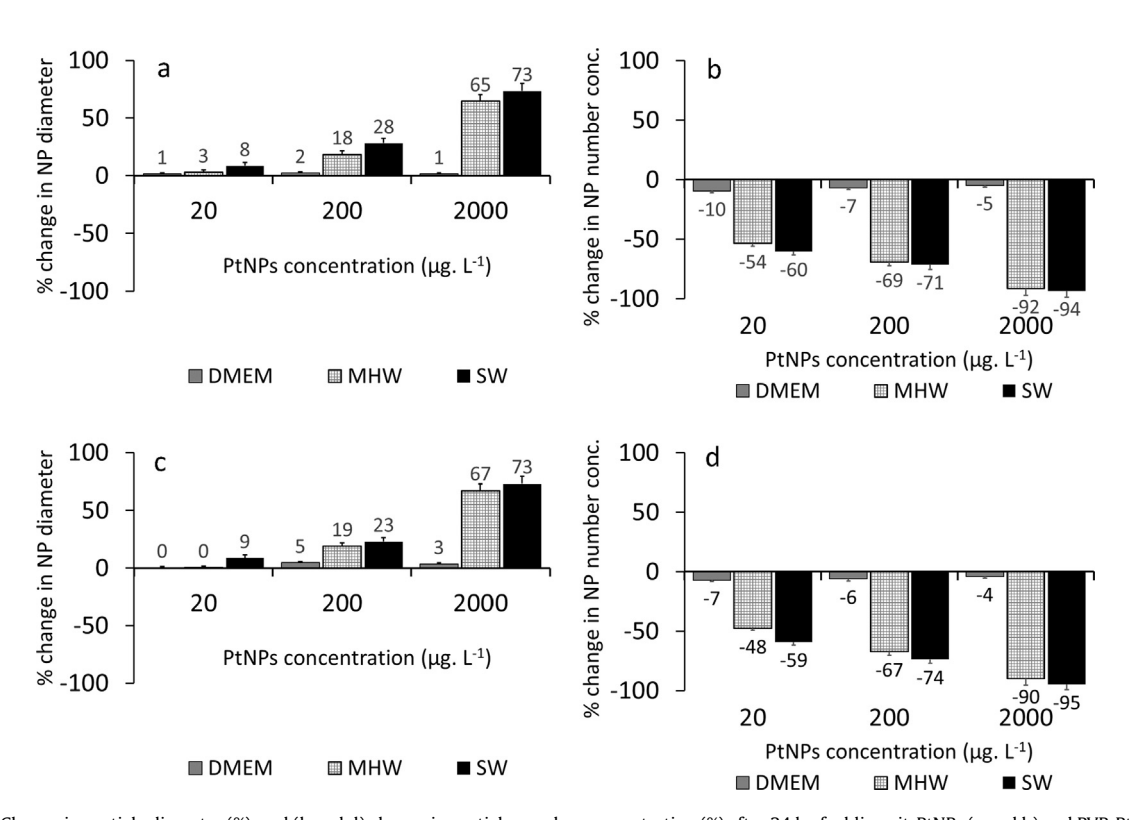
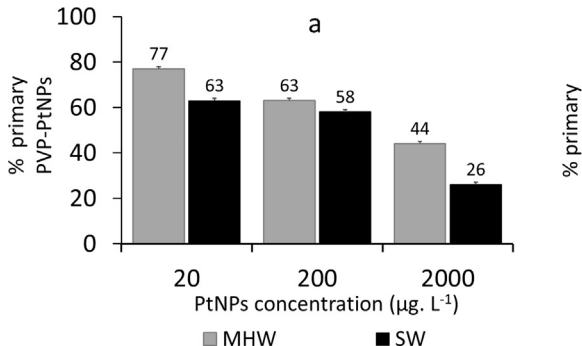


Fig. 5. (a and c) Change in particle diameter (%), and (b and d) change in particle number concentration (%) after 24 h of adding cit-PtNPs (a and b) and PVP-PtNPs (c and d) to DMEM, MHW, and SW. PtNP concentrations were 20, 200, and 2000 μg·L⁻¹. NP diameter and number concentration were measured by sp-ICP-MS.

decrease in AuNP aggregate size concurrent with a decrease in their concentration [69]. Furthermore, the % of primary particles was higher (two-way ANOVA, p < 0.05) for MHW than for SW (Fig. 6) due to the lower ionic strength of MHW compared to SW.

Initial dissolved Pt concentration (at 0 h) was <4% of total PtNPs concentration in all NP suspensions. After 24 h, only 5–15% of PtNPs was dissolved in the different toxicological media (Fig. S13), but these amounts were variable across samples and



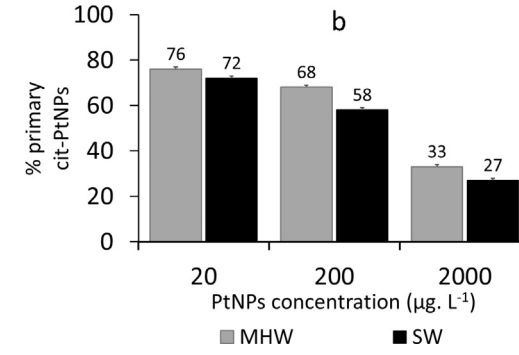


Fig. 6. The percentage of primary particles remaining in suspension after 24 h of adding (a) PVP-PtNPs and (b) cit-PtNPs to moderately hard water (MHW) and 30 ppt synthetic seawater (SW). % of primary PVP-PtNPs was calculated number of primary NPs in the media after 24 h relative to the total number of NPs in original suspension.

not statistically different (two-way ANOVA, p > 0.05). Moreover, we did not observe any differential concentration-dependent dissolution of PtNPs, but a previous study has reported concentration-dependent differential dissolution of AgNPs [73,74]. This is likely attributed to the higher solubility of AgNPs relative to PtNPs (Fig. S14). The aggregation and dissolution behaviors of cit- and PVP-PtNPs were not significantly different. This might be attributed to the partial surface coating of PVP-PtNPs [28]. Thus, both cit- and PVP-PtNPs behaved as charge-stabilized NPs independent of the media ionic strengths evaluated here.

4. Conclusions

A reproducible protocol was developed for the synthesis of monodispersed citrate- and PVP-coated PtNPs of five different size classes, together with a multi-method characterization of NP behavior in relevant biological and toxicological media. In general, the sizes of PtNPs measured using DLS, FIFFF, sp-ICP-MS, TEM and AFM, were all in good agreement whenever PtNP sizes were larger than the size detection limits for each analytical technique. For PVP-coated PtNPs, the thickness of the PVP layer increased with increases in NP size. Observed aggregation of PtNPs was typical of DLVO type aggregation behavior as reported for other types of NPs (e.g., Ag, Au, TiO₂, and iron oxide NPs) [67,75-77]. The critical coagulation concentration of cit-PtNPs was independent of NP size, possibly due to differences in PtNPs surface charge as a function of NP size. The aggregation behavior of PtNPs depends on media composition, NP concentration, and ionic strength. PtNPs tend to remain stable in DMEM regardless of NP surface coating or concentration, whereas they tend to aggregate in MHW and SW for both cit- and PVP-PtNPs. Additionally, PtNPs exhibit an increase in aggregate size concurrent with increases in NP concentration.

At environmentally relevant concentrations (<20 µg L⁻¹), synthesized PtNPs undergo very limited aggregation and/or dissolution and do not change appreciably over time, even in high ionicstrength SW. This reduced PtNPs aggregation behavior is in good agreement with other types of NPs (e.g., iron oxide, AuNPs, AgNPs, and Au@Ag core–shell Nanoparticles) that similarly show reduced aggregation with decreases in concentration [36,59,69]. Taken together, limited aggregation and lack of dissolution at relevant environmental concentrations suggest that PtNPs are an excellent model NP for future fundamental studies of NP environmental transport, fate, deposition and biological uptake. This is because they behave as intact primary NPs in environmental media rather than evolving to dissolved Pt or variably-sized NP aggregates.

The concentration of platinum group elements (PGE) in the environment in the form of nanoparticles has significantly increased over the past decades due to the increased release of Pt from automotive catalytic converters. The limited aggregation

and dissolution of PtNPs at environmentally-relevant particle concentrations suggest that they may persist in the environment and may travel for longer distances in surface waters than other NPs. The concentration-dependent aggregation of PtNPs implies that in (eco)toxicological studies, the nature of PtNPs exposure will change as a function of NP concentration; that is, organisms will likely be exposed to primary nanoparticles at low NP concentrations (<20 $\mu g \cdot L^{-1}$) and predominantly exposed to NP aggregates at higher concentrations. Such concentration-dependent differences in Pt-NPs exposure dynamics should be considered as they are likely to influence NP uptake, elimination and ultimately toxicity as a result of these unique aggregation behaviors.

Conflicts of interest

There are no conflicts of interest to declare.

Acknowledgements

This research was supported by the United States National Science Foundation (NSF1437307) and Virginia Tech National Center for Earth and Environmental Nanotechnology Infrastructure (NanoEarth), a member of the National Nanotechnology Coordinated Infrastructure (NNCI), supported by the Unites States National Science Foundation (ECCS 1542100).

Appendix A. Supplementary material

Supplementary data to this article can be found online at https://doi.org/10.1016/j.jcis.2019.01.036.

References

- [1] PGM mrket report: Summary of platinum supply and demand in 2016, Johnson Matthey PLC, Hertfordshire, 2017.
- [2] A. Dubiella-Jackowska, B. Kudłak, Ż. Polkowska, J. Namieśnik, Environmental fate of traffic-derived platinum group metals, Crit. Rev. Anal. Chem. 39 (4) (2009) 251–271.
- [3] K. Ravindra, L. Bencs, R. Van Grieken, Platinum group elements in the environment and their health risk, Sci. Total Environ. 318 (1) (2004) 1–43.
- [4] J. Pawlak, E. Łodyga-Chruścińska, J. Chrustowicz, Fate of platinum metals in the environment, J. Trace Elem. Med Biol. 28 (3) (2014) 247–254.
- [5] T. Rühle, H. Schneider, J. Find, D. Herein, N. Pfänder, U. Wild, R. Schlögl, D. Nachtigall, S. Artelt, U. Heinrich, Preparation and characterisation of Pt/Al₂O₃ aerosol precursors as model Pt-emissions from catalytic converters, Appl. Catal. B 14 (1) (1997) 69–84.
- [6] K. Folens, T. Van Acker, E. Bolea-Fernandez, G. Cornelis, F. Vanhaecke, G. Du Laing, S. Rauch, Identification of platinum nanoparticles in road dust leachate by single particle inductively coupled plasma-mass spectrometry, Sci. Total Environ. 615 (2018) 849–856.
- [7] B. Bocca, F. Petrucci, A. Alimonti, S. Caroli, Traffic-related platinum and rhodium concentrations in the atmosphere of Rome, J. Environ. Monit. 5 (4) (2003) 563–568

- [8] J. Schäfer, H. Puchelt, Platinum-Group-Metals (PGM) emitted from automobile catalytic converters and their distribution in roadside soils, J. Geochem. Explor. 64 (1) (1998) 307–314.
- [9] O. Morton, H. Puchelt, E. Hernández, E. Lounejeva, Traffic-related platinum group elements (PGE) in soils from Mexico City, J. Geochem. Explor. 72 (3) (2001) 223–227.
- [10] S. Artelt, O. Creutzenberg, H. Kock, K. Levsen, D. Nachtigall, U. Heinrich, T. Rühle, R. Schlögl, Bioavailability of fine dispersed platinum as emitted from automotive catalytic converters: a model study, Sci. Total Environ. 228 (2) (1999) 219–242
- [11] C. Barbante, A. Veysseyre, C. Ferrari, K. Van De Velde, C. Morel, G. Capodaglio, P. Cescon, G. Scarponi, C. Boutron, Greenland snow evidence of large scale atmospheric contamination for platinum, palladium, and rhodium, Environ. Sci. Technol. 35 (5) (2001) 835–839.
- [12] S. Siebel, C. Dammann, W. Hiller, T. Drewello, B. Lippert, Revisiting the head-head dinuclear 1-methyluracil complex of cisplatin: New insights into its solution behavior, Inorganica Chimica Acta 393 (2012) 212–221.
- [13] J. Gao, G. Liang, B. Zhang, Y. Kuang, X. Zhang, B. Xu, FePt@CoS₂ Yolk—shell nanocrystals as a potent agent to kill HeLa cells, J. Am. Chem. Soc. 129 (5) (2007) 1428–1433.
- [14] E. Lamy-Pitara, J. Barbier, Platinum modified by electrochemical deposition of adatoms, Appl. Catal. A 149 (1) (1997) 49–87.
- [15] K.E. Biesinger, G.M. Christensen, Effects of various metals on survival, growth, reproduction, and metabolism of daphnia magna, J. Fish. Res. Board Can. 29 (12) (1972) 1691–1700.
- [16] I. Veltz, F. Arsac, S. Biagianti-Risbourg, F. Habets, H. Lechenault, G. Vernet, Effects of platinum (Pt4+) on Lumbriculus variegatus Muller (Annelida, Oligochaetae): acute toxicity and bioaccumulation, Arch. Environ. Contam. Toxicol. 31 (1) (1996) 63–67.
- [17] M. Książyk, M. Asztemborska, R. Stęborowski, G. Bystrzejewska-Piotrowska, Toxic effect of silver and platinum nanoparticles toward the freshwater microalga Pseudokirchneriella subcapitata, Bull. Environ. Contaminat. Toxicol. 94 (5) (2015) 554–558.
- [18] C. Wei, G.M. Morrison, Platinum in road dusts and urban river sediments, Sci. Total Environ. 146 (1994) 169–174.
- [19] P.V. Asharani, L.W. Yi, Z.Y. Gong, S. Valiyaveettil, Comparison of the toxicity of silver, gold and platinum nanoparticles in developing zebrafish embryos, Nanotoxicology 5 (1) (2011) 43–54.
- [20] M. Tejamaya, I. Romer, R.C. Merrifield, J.R. Lead, Stability of citrate, PVP, and PEG coated silver nanoparticles in ecotoxicology media, Environ. Sci. Technol. 46 (13) (2012) 7011–7017.
- [21] R.C. Merrifield, Z.W. Wang, R.E. Palmer, J.R. Lead, Synthesis and characterization of polyvinylpyrrolidone coated cerium oxide nanoparticles, Environ. Sci. Technol. 47 (21) (2013) 12426–12433.
- [22] R. Behra, B. Wagner, L. Sgier, D. Kistler, Colloidal stability and toxicity of gold nanoparticles and gold chloride on chlamydomonas reinhardtii, Aquat. Geochem. 21 (2) (2015) 331–342.
- [23] T.L. Moore, L. Rodriguez-Lorenzo, V. Hirsch, S. Balog, D. Urban, C. Jud, B. Rothen-Rutishauser, M. Lattuada, A. Petri-Fink, Nanoparticle colloidal stability in cell culture media and impact on cellular interactions, Chem. Soc. Rev. 44 (17) (2015) 6287–6305.
- [24] K.L. Chen, B.A. Smith, W.P. Ball, D.H. Fairbrother, Assessing the colloidal properties of engineered nanoparticles in water: case studies from fullerene C60 nanoparticles and carbon nanotubes, Environ. Chem. 7 (1) (2010) 10–27.
- [25] J. Fabrega, S.N. Luoma, C.R. Tyler, T.S. Galloway, J.R. Lead, Silver nanoparticles behaviour and effects in the aquatic environment, Environ. Int. 37 (2011).
- [26] M. Baalousha, J.R. Lead, Nanoparticle dispersity in toxicology, Nat. Nanotechnol. 8 (2013) 308.
- [27] M. Baalousha, Effect of nanomaterial and media physicochemical properties on nanomaterial aggregation kinetics, NanoImpact 6 (2017) 55–68.
- [28] K. Afshinnia, M. Sikder, B. Cai, M. Baalousha, Effect of nanomaterial and media physicochemical properties on Ag NM aggregation kinetics, J. Colloid Interface Sci. 487 (2017) 192–200.
- [29] N.C. Bigall, T. Härtling, M. Klose, P. Simon, L.M. Eng, A. Eychmüller, Monodisperse platinum nanospheres with adjustable diameters from 10 to 100 nm: synthesis and distinct optical properties, Nano Lett. 8 (12) (2008) 4588-4592
- [30] K.R. Brown, D.G. Walter, M.J. Natan, Seeding of colloidal Au nanoparticle solutions. 2. Improved control of particle size and shape, Chem. Mater. 12 (2) (2000) 306–313.
- [31] M.M. Koebel, L.C. Jones, G.A. Somorjai, Preparation of size-tunable, highly monodisperse PVP-protected Pt-nanoparticles by seed-mediated growth, J. Nanopart. Res. 10 (6) (2008) 1063–1069.
- [32] M. Baalousha, Y. Ju-Nam, P.A. Cole, J.A. Hriljac, I.P. Jones, C.R. Tyler, V. Stone, T. F. Fernandes, M.A. Jepson, J.R. Lead, Characterization of cerium oxide nanoparticles—Part 2: nonsize measurements, Environ. Toxicol. Chem. 31 (5) (2012) 994–1003.
- [33] Gatan Incorporation, Gatan Digital Micrograph Software Instalation Instructions, 2018.
- [34] M. Baalousha, A. Prasad, J.R. Lead, Quantitative measurement of the nanoparticle size and number concentration from liquid suspensions by atomic force microscopy, Environ. Sci.-Process. Impacts 16 (6) (2014) 1338–1347.
- [35] M. Baalousha, J.R. Lead, Rationalizing nanomaterial sizes measured by atomic force microscopy, flow field-flow fractionation, and dynamic light scattering: sample preparation, polydispersity, and particle structure, Environ. Sci. Technol. 46 (11) (2012) 6134–6142.

- [36] R.C. Merrifield, C. Stephan, J. Lead, Determining the concentration dependent transformations of Ag nanoparticles in complex media: using SP-ICP-MS and Au@Ag core-shell nanoparticles as tracers, Environ. Sci. Technol. 51 (6) (2017) 3206–3213
- [37] B. Franze, I. Strenge, C. Engelhard, Single particle inductively coupled plasma mass spectrometry: evaluation of three different pneumatic and piezo-based sample introduction systems for the characterization of silver nanoparticles, J. Anal. At. Spectrom. 27 (7) (2012) 1074–1083.
- [38] F. Laborda, J. Jimenez-Lamana, E. Bolea, J.R. Castillo, Critical considerations for the determination of nanoparticle number concentrations, size and number size distributions by single particle ICP-MS, J. Anal. At. Spectrom. 28 (8) (2013) 1220–1232.
- [39] A. Hineman, C. Stephan, Effect of dwell time on single particle inductively coupled plasma mass spectrometry data acquisition quality, J. Anal. At. Spectrom. 29 (7) (2014) 1252–1257.
- [40] M.D. Montaño, J.W. Olesik, A.G. Barber, K. Challis, J.F. Ranville, Single Particle ICP-MS: advances toward routine analysis of nanomaterials, Anal. Bioanal. Chem. 408 (19) (2016) 5053–5074.
- [41] X. Li, J.J. Lenhart, H.W. Walker, Dissolution-accompanied aggregation kinetics of silver nanoparticles, Langmuir 26 (22) (2010) 16690–16698.
- [42] M. Elimelech, C.R. O'Melia, Kinetics of deposition of colloidal particles in porous media, Environ. Sci. Technol. 24 (10) (1990) 1528–1536.
- [43] OECD, Test No. 202: Daphnia sp. Acute Immobilisation Test, OECD Publishing.
- [44] M.-N. Croteau, S.K. Misra, S.N. Luoma, E. Valsami-Jones, Silver bioaccumulation dynamics in a freshwater invertebrate after aqueous and dietary exposures to nanosized and ionic Ag, Environ. Sci. Technol. 45 (15) (2011) 6600–6607.
- [45] OECD, Organization for Economic Co-operation and Development New Guidance Document on Harpacticoid Copepod Development and Reproduction Test with Amphiascus. Series on Testing and Assessment [Online], 2014, (accessed 2018 18).">http://www.oecd.org/officialdocuments/publicdisplaydocumentpdf/?cote=ENV/JM/MONO(2014)17&doclanguage=en>(accessed 2018 18).
- [46] D.T. Curiel, S. Agarwal, E. Wagner, M. Cotten, Adenovirus enhancement of transferrin-polylysine-mediated gene delivery, Proc. Natl. Acad. Sci. 88 (19) (1991) 8850–8854.
- [47] U.S.E.P. Agency, Methods for Measuring the Acute Toxicity of Effluents and Receiving Waters to Freshwater and Marine Organisms, U.S. EPA, Washington DC. 2002.
- [48] A.D. Pomogailo, G.I. Dzhardimalieva, Reduction of metal ions in polymer matrices as a condensation method of nanocomposite synthesis, in: Nanostructured Materials Preparation via Condensation Ways, Springer, Dordrecht, 2014, pp. 13–89.
- [49] H. Borsook, G. Keighley, Oxidation-reduction potential of ascorbic acid (Vitamin C), Proc. Natl. Acad. Sci. USA 19 (9) (1933) 875–878.
- [50] M. Baalousha, Y. Ju-Nam, P.A. Cole, B. Gaiser, T.F. Fernandes, J.A. Hriljac, M.A. Jepson, V. Stone, C.R. Tyler, J.R. Lead, Characterization of cerium oxide nanoparticles—Part 1: size measurements, Environ. Toxicol. Chem. 31 (5) (2012) 983–993.
- [51] R.F. Domingos, M.A. Baalousha, Y. Ju-Nam, M.M. Reid, N. Tufenkji, J.R. Lead, G. G. Leppard, K.J. Wilkinson, Characterizing manufactured nanoparticles in the environment: multimethod determination of particle sizes, Environ. Sci. Technol. 43 (19) (2009) 7277–7284.
- [52] A. Prasad, J.R. Lead, M. Baalousha, An electron microscopy based method for the detection and quantification of nanomaterial number concentration in environmentally relevant media, Sci Total Environ 537 (2015) 479–486.
- [53] S. Lee, X. Bi, R.B. Reed, J.F. Ranville, P. Herckes, P. Westerhoff, Nanoparticle size detection limits by single particle ICP-MS for 40 elements, Environ. Sci. Technol. 48 (17) (2014) 10291–10300.
- [54] K.J. Wilkinson, É. Balnois, G.G. Leppard, J. Buffle, Characteristic features of the major components of freshwater colloidal organic matter revealed by transmission electron and atomic force microscopy, Colloids Surf., A 155 (2) (1999) 287–310.
- [55] D. Mavrocordatos, D. Perret, G.G. Leppard, Strategies and advances in the characterisation of environmental colloids by electron microscopy Denis mavrocordatos, in: Environmental Colloids and Particles, John Wiley & Sons Ltd., 2007, pp. 345–404.
- [56] J.R. Lead, K.J. Wilkinson, Environmental colloids and particles: current knowledge and future developments, in: Environmental Colloids and Particles, John Wiley & Sons Ltd., 2006, pp. 1–15.
- [57] V. Uskoković, Dynamic light scattering based microelectrophoresis: main prospects and limitations, J. Dispersion Sci. Technol. 33 (12) (2012) 1762– 1786.
- [58] M. Sikder, J.R. Lead, G.T. Chandler, M. Baalousha, A rapid approach for measuring silver nanoparticle concentration and dissolution in seawater by UV–Vis, Sci. Total Environ. 618 (2018) 597–607.
- [59] M. Baalousha, A. Manciulea, S. Cumberland, K. Kendall, J.R. Lead, Aggregation and surface properties of iron oxide nanoparticles: influence of ph and natural organic matter, Environ. Toxicol. Chem. 27 (9) (2008) 1875–1882.
- [60] H. Wang, Y. Wang, Z. Zhu, A. Sapi, K. An, G. Kennedy, W.D. Michalak, G.A. Somorjai, Influence of size-induced oxidation state of platinum nanoparticles on selectivity and activity in catalytic methanol oxidation in the gas phase, Nano Lett. 13 (6) (2013) 2976–2979.
- [61] K.A. Huynh, K.L. Chen, Aggregation kinetics of citrate and polyvinylpyrrolidone coated silver nanoparticles in monovalent and divalent electrolyte solutions, Environ. Sci. Technol. 45 (13) (2011) 5564–5571.

- [62] M. Baalousha, Y. Nur, I. Romer, M. Tejamaya, J.R. Lead, Effect of monovalent and divalent cations, anions and fulvic acid on aggregation of citrate-coated silver nanoparticles, Sci. Total Environ. 454 (2013) 119–131.
- [63] Y.T. He, J. Wan, T. Tokunaga, Kinetic stability of hematite nanoparticles: the effect of particle sizes, J. Nanopart. Res. 10 (2) (2008) 321–332.
- [64] D. Zhou, Z. Ji, X. Jiang, D.R. Dunphy, J. Brinker, A.A. Keller, Influence of material properties on TiO₂ nanoparticle agglomeration, PLoS One 8 (11) (2013) e81239.
- [65] M.J. Mulvihill, S.E. Habas, I. Jen-La Plante, J. Wan, T. Mokari, Influence of size, shape, and surface coating on the stability of aqueous suspensions of CdSe nanoparticles, Chem. Mater. 22 (18) (2010) 5251–5257.
- [66] J. Liu, S. Legros, G. Ma, J.G.C. Veinot, F. von der Kammer, T. Hofmann, Influence of surface functionalization and particle size on the aggregation kinetics of engineered nanoparticles, Chemosphere 87 (8) (2012) 918–924.
- [67] A.M.E. Badawy, T.P. Luxton, R.G. Silva, K.G. Scheckel, M.T. Suidan, T.M. Tolaymat, Impact of environmental conditions (pH, ionic strength, and electrolyte type) on the surface charge and aggregation of silver nanoparticles suspensions, Environ. Sci. Technol. 44 (4) (2010) 1260–1266.
- [68] Y. Li, J.F. Niu, E.X. Shang, J. Crittenden, Photochemical transformation and photoinduced toxicity reduction of silver nanoparticles in the presence of perfluorocarboxylic acids under UV irradiation, Environ. Sci. Technol. 48 (9) (2014) 4946–4953.
- [69] M. Baalousha, M. Sikder, A. Prasad, J. Lead, R. Merrifield, G.T. Chandler, The concentration-dependent behaviour of nanoparticles, Environ. Chem. 13 (1) (2016) 1–3

- [70] E. Fröhlich, G. Bonstingl, A. Höfler, C. Meindl, G. Leitinger, T.R. Pieber, E. Roblegg, Comparison of two in vitro systems to assess cellular effects of nanoparticles-containing aerosols, Toxicol. In Vitro 27–360 (1) (2013) 409–417
- [71] I. Lynch, K.A. Dawson, J.R. Lead, E. Valsami-Jones, Chapter 4-macromolecular coronas and their importance in nanotoxicology and nanoecotoxicology, Front. Nanosci. (2014) 7.
- [72] T. Cedervall, I. Lynch, M. Foy, T. Berggård, S.C. Donnelly, G. Cagney, S. Linse, K.A. Dawson, Detailed identification of plasma proteins adsorbed on copolymer nanoparticles, Angew. Chem. Int. Ed. 46 (30) (2007) 5754–5756.
- [73] M. Sikder, E. Eudy, G.T. Chandler, M. Baalousha, Comparative study of dissolved and nanoparticulate Ag effects on the life cycle of an estuarine meiobenthic copepod, Amphiascus tenuiremis, Nanotoxicology (2018) 1–15.
- [74] M. Sikder, J.R. Lead, G.T. Chandler, M. Baalousha, A rapid approach for measuring silver nanoparticle concentration and dissolution in seawater by UV–Vis, Sci. Total Environ. (2017).
- [75] T. Kim, C.-H. Lee, S.-W. Joo, K. Lee, Kinetics of gold nanoparticle aggregation: experiments and modeling, J. Colloid Interface Sci. 318 (2) (2008) 238–243.
- [76] R.A. French, A.R. Jacobson, B. Kim, S.L. Isley, R.L. Penn, P.C. Baveye, Influence of ionic strength, pH, and cation valence on aggregation kinetics of titanium dioxide nanoparticles, Environ. Sci. Technol. 43 (5) (2009) 1354–1359.
- [77] T. Phenrat, N. Saleh, K. Sirk, R.D. Tilton, G.V. Lowry, Aggregation and sedimentation of aqueous nanoscale zerovalent iron dispersions, Environ. Sci. Technol. 41 (1) (2007) 284–290.